

Fully Automatic Deep Learning Pipeline for Whole Slide Image Quality Assessment

Falah Jabar, Lill-Tove Rasmussen Busund, Biagio Ricciuti, Masoud Tafavvoghi, Mette Pøhl, Sigve Andersen, Tom Donnem, David J. Kwiatkowski, Mehrdad Rakaee

Abstract—In recent years, the use of deep learning (DL) methods, including convolutional neural networks (CNNs) and vision transformers (ViTs), has significantly advanced computational pathology, enhancing both diagnostic accuracy and efficiency. Hematoxylin and Eosin (H&E) Whole Slide Images (WSI) plays a crucial role by providing detailed tissue samples for the analysis and training of DL models. However, WSIs often contain regions with artifacts such as tissue folds, blurring, as well as non-tissue regions (background), which can negatively impact DL model performance. These artifacts are diagnostically irrelevant and can lead to inaccurate results. This paper proposes a fully automatic supervised DL pipeline for WSI Quality Assessment (WSI-QA) that uses a fused model combining CNNs and ViTs to detect and exclude WSI regions with artifacts, ensuring that only qualified WSI regions are used to build DL-based computational pathology applications. The proposed pipeline employs a pixel-based segmentation model to classify WSI regions as either qualified or non-qualified based on the presence of artifacts. The proposed model was trained on a large and diverse dataset and validated with internal and external data from various human organs, scanners, and H&E staining procedures. Quantitative and qualitative evaluations demonstrate the superiority of the proposed model, which outperforms state-of-the-art methods in WSI artifact detection. The proposed model consistently achieved over 95% accuracy, precision, recall, and F1 score across all artifact types. Furthermore, the WSI-QA pipeline shows strong generalization across different tissue types and scanning conditions.

Index Terms— Computational Pathology, Whole Slide Images, Deep Learning, Artifacts Detection, Whole Slide Images Quality Assessment.

This research is supported by The Norwegian Cancer Society (grant 273190-13 2024) and the Northern Norway Regional Health Authority (grant HNF1660-23). The funders had no role in the design and conduct of the study; and decision to submit the manuscript for publication. (Corresponding author: Falah Jabar).

Falah Jabar is with the Department of Clinical Pathology, University Hospital of North Norway, Tromsø, Norway (e-mail: falah.rahim@unn.no).

Lill-Tove Rasmussen Busund is with the Department of Clinical Pathology, University Hospital of North Norway, Tromsø, Norway, and Department of Medical Biology, UiT The Arctic University of Norway, Tromsø, Norway (e-mail: lill.tove.rasmussen.busund@unn.no).

Biagio Ricciuti is with the Lowe Center for Thoracic Oncology, Dana-Farber Cancer Institute, Harvard Medical School, Boston, USA (e-mail: biagio_ricciuti@dfci.harvard.edu).

Masoud Tafavvoghi is with the Department of Community Medicine, UiT The Arctic University of Norway, Tromsø, Norway (e-mail: masoud.tafavvoghi@uit.no).

Mette Pøhl is with the Department of Oncology, Copenhagen University Hospital, Rigshospitalet, Copenhagen, Denmark (e-mail: mette.poehl@regionh.dk).

I. INTRODUCTION

In recent years, the integration of deep learning (DL) pipelines has improved diagnostic accuracy and efficiency, leading to better patient outcomes. DL models are used for detection, classification, and outcome prediction in various cancer types [1][2][3]. Recent advances in whole slide imaging technologies enable the capture of gigapixel WSI of tissue slides, which contain detailed sections of tissue specimens. These WSI undergo preprocessing before being utilized to train DL pipelines. Normally, the preprocessing includes [4][5]:

- WSI tiling - The WSIs are gigapixel images that cannot be processed or fed to the DL pipelines at once. Therefore, tiling is often used as a preprocessing step to break down these large images into smaller image tiles.
- WSI color normalization/ augmentation - The WSI obtained from different scanners and/or due to differences in staining processes can result in significant color variations. Typically, these color variations are addressed using color normalization or color augmentation techniques.
- WSI quality assessment (WSI-QA) - The WSIs have regions with background and artifacts such as tissue folds and blurring, which are introduced during slide preparation and scanning. The background and artifacts need to be excluded.

Typically, during diagnosis the pathologists ignore WSI regions that have folding or uneven surfaces (Fig. 1a-b) and blurring (Fig. 1c-d) artifacts. Tissue folds occur when a thin tissue slice

Sigve Andersen is with the Department of Clinical Medicine, UiT The Arctic University of Norway, Tromsø, Norway, and Department of Oncology, University Hospital of North Norway, Tromsø, Norway (e-mail: sigve.andersen@uit.no).

Tom Donnem is with the Department of Clinical Medicine, UiT The Arctic University of Norway, Tromsø, Norway, and Department of Oncology, University Hospital of North Norway, Tromsø, Norway (e-mail: tom.donnem@uit.no).

David J. Kwiatkowski is with the Department of Medicine, Brigham and Women's Hospital, Harvard Medical School, Boston, USA, and Department of Medical Oncology, Dana-Farber Cancer Institute, Boston, USA (e-mail: dkwiatkowski@mgb.org).

Mehrdad Rakaee is with the Department of Clinical Pathology, University Hospital of North Norway, Tromsø, Norway, and Department of Cancer Genetics, Oslo University Hospital, Oslo, Norway (e-mail: mehrdad.rakaee@uit.no).

The source code is available on [GitHub](#), and the supplementary materials are available on [SupplementaryMaterial](#).

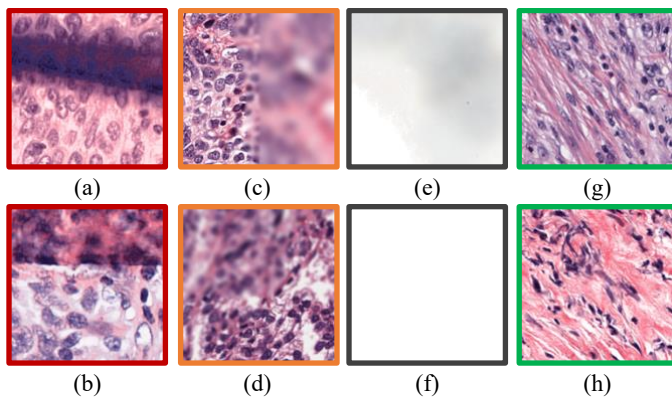


Fig. 1. Examples of image tiles obtained from different WSIs: (a)-(b) image tiles with tissue fold; (c)-(d) image tiles with blur; (e)-(f) image tiles without tissue regions (background); (g)-(h) artifact-free image tiles.

folded onto itself, and blurring occurs when tissue is out of focus during scanning. Additionally, the WSIs often include non-tissue regions (background) as shown in Fig. 1e-f, which are also ignored by pathologists [2]. As can be seen in Fig. 1a-b, tissue folds appear (big darker regions) unevenly across the image tile, affecting some regions while leaving others intact. The strength of this artifact can vary, some regions appearing darker than other regions. This variability is also seen for blurring artifact (Fig. 1c-d), where certain regions of the image tile are more blurred than others. In addition, non-tissue regions (background) may appear in various locations, such as outside or between tissue regions. Typically, the background outside tissue regions appears white and can be detected and excluded using simple image segmentation techniques, such as Otsu's method [5][6]. However, depending on slide preparation and WSI scanners, the background between tissue regions may appear with different colors and intensities (as shown in Fig. 1e-f), making it difficult for basic image segmentation methods to identify these regions.

The variations in color and intensity at the pixel level make it quite challenging to detect artifacts in WSIs. Including such artifacts in the development of any DL pipelines can significantly degrade the performance (e.g., overfitting, underfitting, poor generalization), and possibly lead to incorrect prediction [6][7]. Therefore, the WSI-QA is an essential preprocessing step. Manually selecting image tiles is impractical due to the need to visually evaluate thousands/millions of image tiles per WSI, making it extremely time-consuming for pathologists. In this context, the main objective of this paper is to develop a fully automatic WSI-QA pipeline to select qualified image tiles (those contain minimum artifacts and an acceptable amount of tissue) before utilizing for DL pipelines.

The main contributions of this paper are as follows:

- Development of a large and diverse dataset of WSI artifacts, including tissue folds, blurring, and background, obtained from multiple WSIs and annotated by experts.
- Development of an efficient procedure that allows for pixel-based annotation in WSIs, making the labeling process more precise and suitable for deep learning applications.

- Development of a fully automatic preprocessing DL pipeline to quantify WSI artifacts and background, assessing the quality of image tiles by classifying them into two classes, qualified image tiles and non-qualified image tiles (see Fig. 1). The DL pipeline was made available on [GitHub](#).

- Conduct an intensive qualitative and quantitative evaluation over internal and external datasets including WSIs obtained from different human organs and scanners, and assess the performance of the proposed DL pipeline against the state-of-the-art pipelines.

The rest of this paper is organized as follows: Section II reviews related work; Section III describes the annotation procedure and datasets used in this study; Section IV details the proposed WSI-QA pipeline; Section V presents the performance evaluation results; and finally, Section VI concludes the paper with future work directions.

II. RELATED WORK

Most work on WSI preprocessing steps focus on addressing WSI color variations, with the use of color normalization and/or augmentation techniques [2][8][9]. However, there are not many work dedicated to WSI-QA, particularly artifacts detection, which is essential to ensure only high-quality and relevant histological data are used in DL pipelines developed for diagnostic purposes. A major challenge in this area is the lack of publicly available, reliable, and diverse datasets for WSI artifacts, making it difficult to develop robust pipelines for artifact detection.

Early work on artifact detection rely on traditional image processing techniques, such as feature extraction and color processing. In [10][11], a combination of image features such as contrast, gradient, and local statistics, was used to detect blurry regions in WSIs. Similarly, in [12], image noise information and sharpness were combined to detect blurring in WSIs. In [13][14], color information is used to detect folded regions in WSIs. In [13], the red, green, and blue (RGB) channels of the WSIs are transformed to hue, saturation, and intensity (HSI) and then the k-means clustering technique is applied to identify the folded regions. In [14], assuming the folded regions are darker than other regions, the color enhancement method was proposed to identify the folded regions in WSIs. In [15], adaptive thresholding segmentation is used to identify and discard folded tissues in WSIs. Similarly, in [16] image color and texture with the k-means clustering method were used to classify diagnostically relevant vs. non-relevant regions in WSIs (e.g., folds and white background). Although these approaches laid a foundation for WSI artifact detection, they are limited in handling WSIs with varying colors, staining methods, scanners, or those of different histologies.

In [17], HistoQC, an open-source software for WSI-QA, was developed to assist pathologists in identifying and quantifying artifacts in WSIs. The HistoQC uses a combination of image processing techniques and supervised classifier to detect artifacts such as blurring, pen markers, tissue folds, and white backgrounds. The WSI and detected artifacts are presented to

pathologists via an interactive graphical user interface. However, a key limitation is that final results still require pathologist interactions, limiting full automation. The work in [7], investigated the impact of WSI artifacts on ML algorithms developed for digital pathology. The study concluded that the presence of artifacts may negatively influence the performance of these algorithms. However, no algorithm was developed to automate the artifact detection.

To address the limitations of previous work, recent studies have adopted DL approaches. In [18], multiple DL pipelines were trained and compared for detecting blurred regions in WSIs. The study found that DL-based methods obtained significantly higher accuracy than traditional image processing techniques. In [19], ConvFocus quantifies the severity and localizes blurry regions in WSIs. Similarly, in [20], multiple DL pipelines and binary classifiers were trained and compared for detecting folded regions in WSIs. In [21], a vision transformer is trained to detect air bubbles. In [22], a DL pipeline is proposed to assess the impact of color normalization over blood and fold tissue detection. All these methods relied on training a single pipeline to classify one or two artifacts against an artifact-free class. In addition, these models are trained on a small dataset that may suffer from poor generalization.

In more recent work, a multiclass DL pipeline was proposed in [23] to predict the presence of artifacts in WSI. Similarly, in [24], instead of a multiclass, several binary DL pipelines were trained, and their outputs were combined to predict the presence of artifacts in WSIs. The primary drawback of the recent approach is that it was trained on a small, single-cohort dataset consisting exclusively of bladder images from one scanner, which may limit its ability to generalize and perform well on unseen data [24].

The existing methods exhibit several key limitations, summarized as follows:

- **Background detection:** Most work relies on the Otsu thresholding method to identify non-tissue regions. While this method may perform well for detecting background outside tissue regions, it does not perform well for identifying background between tissue regions due to color variations [23][24][25][26].
- **Tile-level classification:** Current methods are mainly tile-based classifiers based on the presence of artifacts. If any artifacts are detected, even in a small region of a few pixels, the entire tile is marked as unqualified, possibly discarding valuable information such as critical tumor regions.
- **Lack of dataset diversity:** Many methods are trained on small, limited datasets that focus on a specific magnification (e.g., 20x), neglecting data from different magnifications and reducing generalizability across various WSI magnifications.

To address these challenges, the proposed preprocessing DL-based pipeline is trained on a diverse dataset and uses pixel-based segmentation to classify image tiles into two categories: qualified and non-qualified. The model was independently validated on external datasets, representing different human organs and scanners, and its performance was benchmarked against state-of-the-art methods.

III. DATA MATERIALS

This section describes the creation of a diverse dataset for model development, an external dataset to benchmark performance against state-of-the-art methods, and the proposed procedure for WSI annotation.

A. Development Dataset

H&E slides were collected from multiple centers with different staining procedures. The dataset includes: (1) 446 WSIs of metastatic non-small cell lung cancer (NSCLC) patients from the Dana-Farber Cancer Institute (DFCI), of which 66 had artifacts [25] and (2) 453 WSIs of NSCLC patients from a Scandinavian multi-institutional clinical trial (TNM-I), of which 73 had artifacts [26]. The WSIs from DFCI were scanned using the Aperio ScanScope AT scanner at 0.5 $\mu\text{m}/\text{px}$ (20x magnification), while the WSIs from TNM-I were scanned using the 3DHistech scanner at 0.25 $\mu\text{m}/\text{px}$ (40x magnification). In total, 24,942 tiles were generated, with the following distribution: 9,828 artifact-free (qualified tissue) tiles, 7,334 tiles with folding, and 7,780 tiles with blurring (see Fig.S2-a in the supplementary materials). Additionally, 1000 background tiles from various WSIs were included to ensure the model can detect backgrounds with varying colors (see Fig.S2-c in the supplementary materials). The dataset was built using the procedure described in section III.C. All the patients were consented and the data collection was ethically approved by the Institutional Review Board at each participating institute: DFCI-2021P000557; TNM-I-REK2016/2054.

B. External Validation Dataset

This external dataset includes 18 H&E-stained WSIs, which had artifacts, including six different organs: brain, breast, bladder, lung, liver, and kidney, obtained from the TCGA dataset [27]. Each organ is represented by three WSIs (3 WSIs per organ, totaling 18). The brain and bladder WSIs were scanned at 0.5 $\mu\text{m}/\text{px}$ (20x magnification), while the remaining organs were scanned at 0.25 $\mu\text{m}/\text{px}$ (40x magnification). In total, 10,701 tiles were generated, with the following distribution: 3117 artifact-free (qualified tissue) tiles, 1350 tiles with folding, and 6243 tiles with blurring (see Fig.S2-b in the supplementary materials). The dataset was built using the procedure described in the following section.

C. Annotation Procedure

Supervised pixel-based segmentation requires ground truth data where each pixel is accurately labeled, making the WSI annotation task challenging and time-consuming. Consider the WSI-ROI (as shown in Fig. 2) as a 2D grid of pixels, I , where each pixel is indexed by (i, j) and represented by three color values (R, G, B). The set of labels is $L = \{l_k\}$, where $k = 0, 1, 2, \dots, M$, and M is the number of distinct labels. The objective is to assign a label l_k to each pixel within in a region indexed by r , where $r = 1, 2, 3, \dots, R$, and R is the number of distinct regions. For example, label 0 is assigned to all pixels in the background regions. Thus, $I(i, j)_r = l_k$, where $l_k \in L$. To achieve this, an annotation procedure was proposed to label WSI pixels specifically for segmentation tasks.

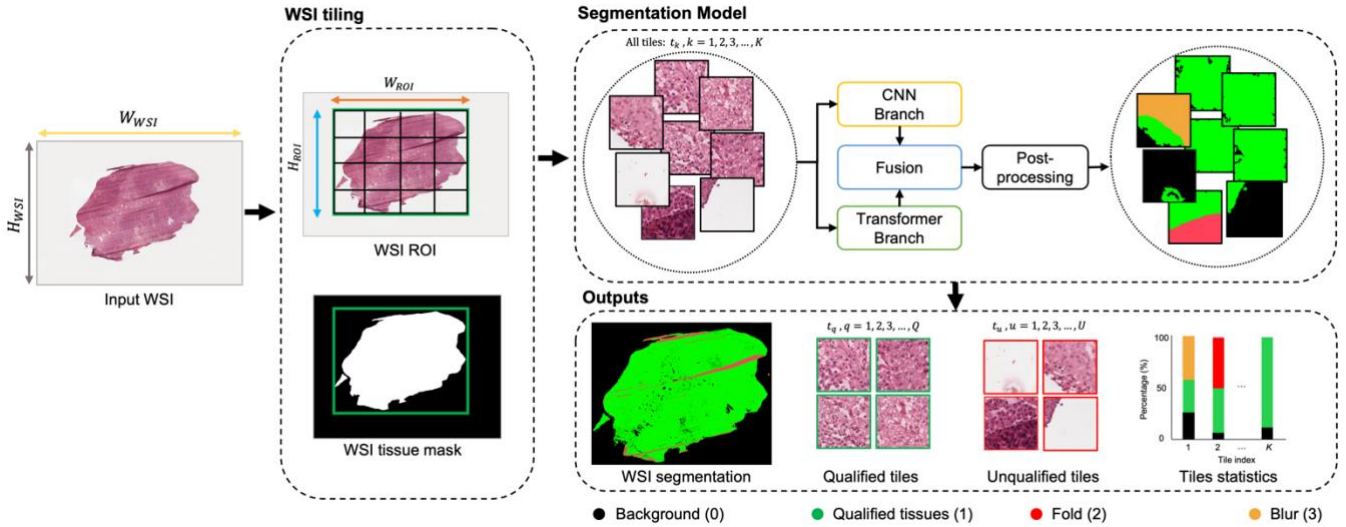


Fig. 2. Proposed Whole Slide Image Quality Assessment (WSI-QA) pipeline.

A schematic overview of the annotation process is provided in Fig.S1 of the supplementary materials, and is summarized as follows:

- **Annotation:** Set magnification in QuPath software [28] to a minimum of 20x. Manually annotate regions with artifacts (e.g., folds or blurring) within the QuPath environment to ensure precise labeling. Next, tile the annotated regions of WSI to generate tiles from regions containing artifacts. Each tile has a resolution of $(H_t, W_t, 3)$ pixels, where 3 represents the (R, G, B) channels. The generated tiles include both unannotated regions (qualified tissue and background) and annotated regions (folding and blurring). For each tile, a corresponding 2D segmentation mask is generated with the same (H_t, W_t) . In the mask, unannotated regions are labeled as 0, folding is labeled as 2, and blurring is labeled as 3.

- **Post-processing:** Using the information in the segmentation mask, the unannotated regions in each RGB tile are separated from the annotated regions. The unannotated regions are further processed to distinguish background from qualified tissue by applying the background segmentation technique proposed in [29]. In short, the RGB image tile is converted to hue, saturation, and lightness (HSL) color space. Then, color thresholding is applied to separate the background from the tissue regions. The final segmentation mask is then generated, where the background is labeled as 0, qualified tissue as 1, folding as 2, and blurring as 3 (see Fig.S2-c of the supplementary materials).

This procedure is adaptable to various WSI segmentation tasks (e.g., tissue type segmentation), not just artifact segmentation.

IV. WSI-QA PIPELINE

This section describes the proposed Whole Slide Image Quality Assessment (WSI-QA) pipeline, including its main architecture, implementation, and training procedure. The WSI-QA pipeline is presented in Fig. 2. First, the region of interest (WSI-ROI) is identified and divided into smaller image tiles, which are then fed to the DL segmentation model, generating pixel-based tiles segmentation. The segmented tiles are then

post-processed, allowing for the classification of tiles into two categories: qualified (tiles with a minimum amount of background and artifacts) and unqualified tiles (tiles with artifacts and/or background). Additionally, the model generates a segmentation for the entire WSI and also provides statistics on the tile segmentations. A detailed explanation of each step and the model training process is provided below.

A. WSI Tiling

To exclude background, the WSI with resolution (H_{WSI}, W_{WSI}) pixels is first down sampled to (5000, 5000) pixels, and then Otsu segmentation [30] is applied to generate a tissue mask, separating tissue regions (labeled as 255) from the background (labeled as 0), as shown in Fig. 2. Small tissue regions that have less than 25 pixels are removed [31], followed by a dilation morphological operation [32], using 8-neighbor connectivity to expand the tissue borders. The identified tissue regions (WSI-ROI), indicated by the green rectangle in Fig. 2, have a resolution of (H_{ROI}, W_{ROI}) pixels. The tiling is then performed over WSI-ROI, with each tile having a resolution of (H_t, W_t) pixels, and indexed as t_k , where $k = 1, 2, 3, \dots, K$, with K being the total number of tiles. To speed up the process, tiling is performed using parallel processing [33].

B. Segmentation Model

The segmentation model is a dual-branch hierarchical global-local fusion network based on the work proposed in [34]. Briefly, it combines a global encoder, Swin Transformer – a vision transformer that extracts global image features – and a local encoder, ConvNeXt – a convolutional neural network that extracts local image features. This model is designed to handle segmentation tasks in WSIs. The Swin Transformer focuses on global image structure, while ConvNeXt refines local details, ensuring high segmentation accuracy. Details about model architecture can be found in [34]. The model is trained on the development dataset described in section III.A, with the training procedure explained in the following section.

The input tiles, each with a resolution of 270 by 270 pixels, are fed into the segmentation model, which generates pixel-based

segmentation for each tile, assigning labels to each pixel: 0 for background (black color), 1 for qualified tissue (green color), 2 for fold (red color), and 3 for blurring (orange color), as shown in Fig. 2. In post-processing step, the WSI segmentation is obtained by merging all individual tile segmentations. Additionally, statistics on the tile segmentations – such as percentage of artifacts, background, and qualified tissues (artifact-free) – are generated, to quantify artifacts, background, and qualified tissue in WSI. In the tile segmentation mask, small background regions (holes with less than 25 pixels) are closed, as such small background regions are not significant enough to impact the overall analysis. Finally, the tiles are classified into two groups based on the amount of existing artifacts and/or background:

- If the amount of background (in pixels) $> T_{bc}$, the tile is classified as unqualified (background). The T_{bc} is the background threshold parameter that controls how much background is tolerated in the tiles (e.g., 50%).
- If the amount of background (in pixels) $< T_{bc}$, but the amount of blurring and/or folding (in pixels) $> T_{ar}$, the tile is also classified as unqualified (fold or blur). The T_{ar} is the folding and blurring threshold parameter that controls how much folding and/or blurring artifacts are tolerated in the tiles (e.g., 10%).
- If the amount of background (in pixels) $< T_{bc}$, and the amount of blurring and/or folding (in pixels) $< T_{ar}$, the tile is classified as qualified (artifact-free).

The tiles in the qualified group are indexed as t_q , where $q = 1, 2, 3, \dots, Q$, with Q being the total number of tiles in the group. The tiles in the unqualified group are indexed as t_u , where $u = 1, 2, 3, \dots, U$, with U being the total number of tiles in the group, where $Q + U = K$.

C. Model Training

The dataset was randomly split, 87% for training and 13% for testing. Detailed information regarding the dataset split can be found in Fig.S2-a in the supplementary materials. The Adam optimizer was employed to minimize the loss function and achieve optimal performance. Various batch sizes and learning rates were tested during the optimization process. Specifically, learning rates were evaluated in the range of 10^{-2} to 10^{-4} , and batch sizes of 16, 32, and 64 were tested. The optimal configuration that better minimizes the loss function was found to be a batch size of 64 and a learning rate of 10^{-3} .

Throughout the training process, Weights and Biases (WandB), a widely used tool for tracking, visualizing, and optimizing machine learning experiments [35], was employed to monitor the model’s progress. To enhance the model’s generalization, various data augmentation was applied, including horizontal and vertical flips and color augmentation [36]. Horizontal and vertical flips were used to increase spatial diversity, while color augmentations (brightness = 0.5, contrast = 0.5, saturation = 0.5, hue = 0.5) were applied to improve robustness against color variations. Initial parameter settings for the network were based on guidance from [34]. The model was trained for 150 epochs, as increasing the number of epochs beyond this did not lead to

further performance improvements. The training was performed on a system equipped with an NVIDIA A100 GPU (80GB of memory) running CUDA version 12.2. The system also featured an Ubuntu operating system (version 20.4), a 40-core CPU, and 512GB of RAM. The model is publicly available on [GitHub](#).

V. PERFORMANCE EVALUATION

This section presents quantitative and qualitative evaluations of the proposed WSI-QA pipeline, comparing it to state-of-the-art methods. The performance evaluation was conducted using the test set from the development dataset as well as an external validation set. Both sets consist of unseen data that were never used during the training of the model, ensuring an unbiased evaluation of the proposed pipeline’s performance. For the proposed WSI-QA pipeline, as described in section IV, tiles can be classified based on specific thresholds: a background threshold of $T_{bc} = 50\%$, meaning any tile with 50% or more background is considered as a background tile, and a folding and blurring threshold of $T_{ar} = 10\%$, meaning any tile with more than 10% blurring or folding is considered as a blurred or folded tile. The state-of-the-art methods used for comparison include four recently proposed pipelines in [23]: two pipelines of Mixture of Experts (MoE) — one based on convolutional neural networks, referred to as MoE-CNN, and the other based on vision transformers, referred to as MoE-ViT — as well as two multiclass pipelines, one based on CNNs referred to as multiclass-CNN and the other based on ViTs referred to as multiclass-ViT. To ensure a fair comparison and to accurately evaluate the performance of the proposed WSI-QA pipeline against the benchmark methods for each artifact, the following classes were considered: artifact-free, fold, and blur. Quantitative metrics, including total accuracy (Acc), precision, recall, and F1 score, were used to evaluate performance [23][37].

A. Quantitative Evaluation

Fig. 3 shows the performance metrics for both proposed and benchmark pipelines on the development dataset (test set) and external validation dataset. Additionally, confusion matrices for each model and dataset are available in Table S.1 of the supplementary materials. The following conclusions can be drawn:

- **Proposed:** The proposed model achieved the best performance across all artifact types (artifact-free, blur, fold) in both the development and external datasets. It achieved precision, recall, and F1 scores, and total accuracy above 95%, indicating its robustness and strong ability to generalize to unseen data. See the confusion matrixes in Table S.1 of the supplementary materials.
- **MoE-CNN:** This pipeline was selected as the best in [23], and performed significantly poorer than the proposed pipeline, with a total accuracy of 74% on the development dataset and 70% on the external validation dataset. For the development dataset, the model achieved an average precision of 74%, recall of 70%, and an F1-score of 71% across the three classes. In the external dataset, the average precision was 68%, recall 72%, and F1-

score 65%. As shown in Fig. 3, the model struggles particularly with the fold class, indicating poor performance in handling this specific artifact type.

- **MoE-ViT**: This pipeline displays a clear gap in performance between the development and external datasets, achieving 52% total accuracy in the development dataset but improving to 76% in the external validation dataset. For the development dataset, the model achieved an average precision of 58%, recall of 59%, and an F1-score of 52% across the three classes. In the external dataset, the average precision was 71%, recall 79%, and F1-score 72%. This model shows weak performance in the artifact-free and fold classes within the development dataset but demonstrates better results in the external dataset. This inconsistency across different artifact types indicates that the model struggles with generalization, particularly when handling varied types of data.

- **Multiclass-CNN**: This pipeline performs similarly to the MoE-CNN in the development dataset, with a total accuracy of 75%, but shows better performance in an external dataset, achieving a total accuracy of 83%. For the development dataset, the model achieved an average precision of 82%, recall of 70%, and an F1-score of 69% across the three classes. In the external dataset, the average precision was 82%, recall 73%, and F1-score 74%. However, as seen in Fig. 3, like MoE-CNN, struggles significantly with the fold class, indicating a weakness in handling this particular artifact type.

- **Multiclass-ViT**: This model shows slightly better performance than MoE-ViT on the development dataset, achieving a total accuracy of 58%, performing better in the artifact-free class but worse in the blur class. However, it performs lower than MoE-ViT on the external validation dataset, with a total accuracy of 67%. For the development dataset, the model achieved an average precision of 69%, recall of 53%, and an F1-score of 53% across the three classes. In the external dataset, the average precision improved to 76%, with recall at 69% and an F1-score of 67%. However, like MoE-ViT, its inconsistent performance across different artifact types indicates that the model struggles with generalization, particularly when handling diverse data.

The external validation dataset includes WSI images from six different organs: bladder, brain, breast, kidney, liver, and lung. To evaluate the performance of the proposed WSI-QA pipeline across these organs, the performance metrics for each organ are presented in Fig. 4, alongside the best state-of-the-art method (MoE-CNN)[23]. The proposed model outperforms MoE-CNN across all organ types. It consistently achieves performance for all metrics above 95% across all organs. In contrast, MoE-CNN shows noticeable variation in performance across different organ types, with total accuracy ranging from 52% (liver) to 80.9% (brain). This indicates that the MoE-CNN model cannot generalize well for different tissue types. Furthermore, it has poor performance for fold class. The confusion matrix for each organ and both proposed and MoE-CNN is provided in Table S.2 in the supplementary materials.

B. Qualitative Evaluation

Fig. 5 are representative tiles to visually compare the artifact segmentation performance between the proposed WSI-QA pipeline and the state-of-the-art method, MoE-CNN, across six different organs (bladder, brain, breast, kidney, liver, lung) and background-only regions. Note that the proposed WSI-QA uses pixel-based segmentation, where each pixel is individually labeled, leading to more precise segmentation. In contrast, MoE-CNN performs tile-based segmentation, meaning that if a tile is classified as fold, all pixels within that tile are assigned the same label, potentially leading to less precise segmentation results. Additionally, in Fig. 5 the ground truth classification for each tile is provided, allowing for a direct comparison of model performance.

The proposed WSI-QA pipeline shows a high level of accuracy in both artifact segmentation and classification across all organ tiles and background images. The predicted classification labels match the ground truth for all tiles, demonstrating the model's ability to correctly distinguish between qualified and unqualified tiles. In contrast, MoE-CNN lacks precise artifact segmentation as it operates on tiles rather than individual pixels, resulting in less accurate classification. Additionally, many qualified tiles are incorrectly classified as containing folds (see Fig. 5 - brain, kidney, liver, lung). This misclassification likely occurs because certain cell regions have colors similar to fold regions, causing the model to label the entire tile as a fold, even though it contains only normal cells and no actual fold artifacts. The proposed WSI-QA pipeline accurately identifies all background-only tiles as unqualified, matching the ground truth labels. In contrast, MoE-CNN misclassifies some background-only tiles, particularly those with a reddish color, as qualified. This leads to tiles without tissue being mistakenly classified as suitable for analysis. Additional WSI segmentations produced by the proposed WSI-QA pipeline and MoE-CNN are provided in Fig. S3 and S4 of the supplementary materials. Fig. 5, along with Fig. S3 and S4 in the supplementary materials, demonstrate the superior artifact segmentation performance of the proposed WSI-QA pipeline compared to MoE-CNN. The pixel-based approach of the proposed model leads to more precise and accurate classifications.

It is worth mentioning that the proposed WSI-QA pipeline can have two potential applications: i) as a preprocessing tool to clean and prepare data for deep learning models and ii) as an integrated component in computational pathology systems.

VI. CONCLUSION

This paper proposes a fully automated deep learning pipeline for Whole Slide Image Quality Assessment (WSI-QA) that addresses key challenges in histopathology, particularly the detection and exclusion of WSI regions with artifacts such as tissue folds, blurring, and background. By employing a dual-branch hierarchical global-local fusion network combining convolutional neural networks and vision transformer, the proposed WSI-QA model demonstrates superior performance in identifying WSI regions with artifacts. Both quantitative and qualitative evaluations on internal and external diverse datasets, which include WSIs from different tissue types and scanning

conditions, show that the model consistently achieves over 95% accuracy, precision, recall, and F1 scores across all artifact types, significantly outperforming state-of-the-art methods. The experimental results further demonstrate that the pixel-based segmentation approach of the WSI-QA pipeline enables more precise classification of artifact regions compared to tile-based methods, ensuring higher segmentation quality. In future work, addressing pen markings, a common artifact often introduced by pathologists during slide review, will be a

key focus. These pen markings can cover important WSI tissue regions, potentially leading to misinterpretations in automated analysis. While pen markings can be detected and removed, this task presents unique challenges as they vary in size, color, and location. Tackling this issue requires specialized techniques beyond conventional artifact detection. One promising approach is the use of generative AI models, such as Generative Adversarial Network [38] or diffusion model [39], trained specifically to clean WSI regions with pen markings.

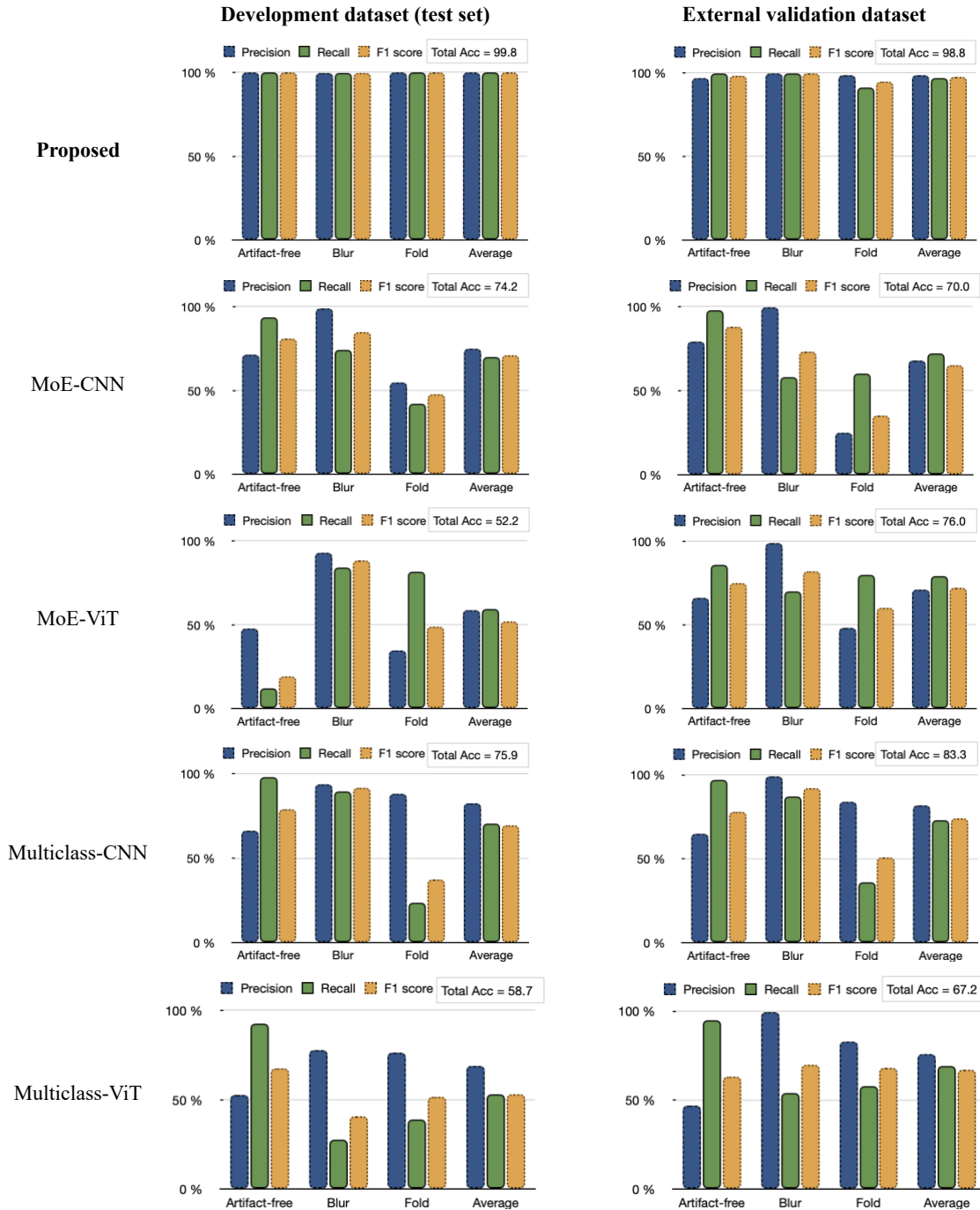


Fig. 3. Comparing the performance of the proposed WSI-QA pipeline with the state-of-the-art methods. The left column shows performance metrics on the development dataset (test set), while the right column presents performance metrics on the external validation dataset. The last three columns represent the average performance across artifact-free, blur, and fold categories.

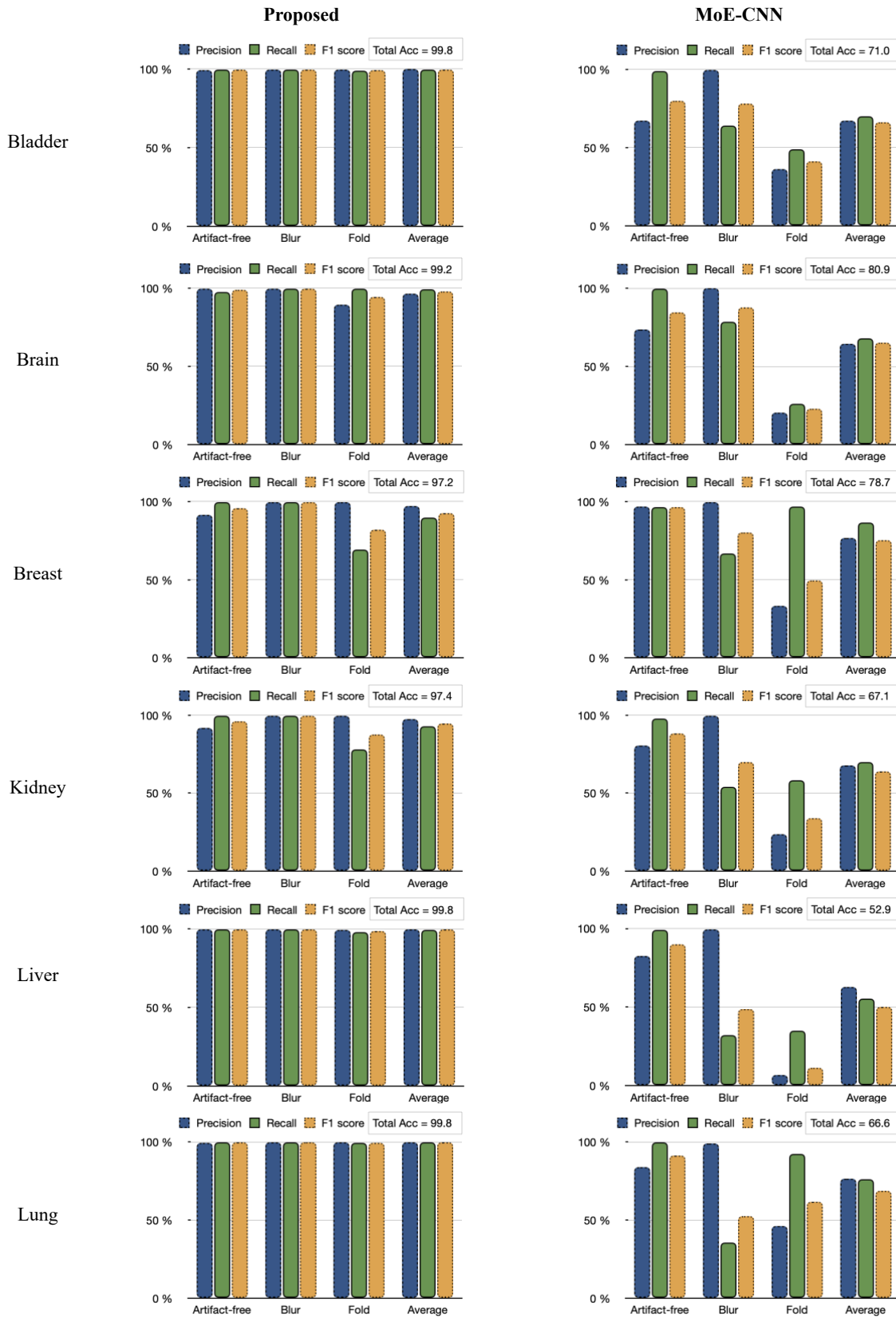


Fig. 4. Comparing the performance of the proposed WSI-QA pipeline with the best state-of-the-art method (MoE-CNN) on the external validation dataset, evaluating results for each organ. The last three columns represent the average performance across artifact-free, blur, and fold categories.

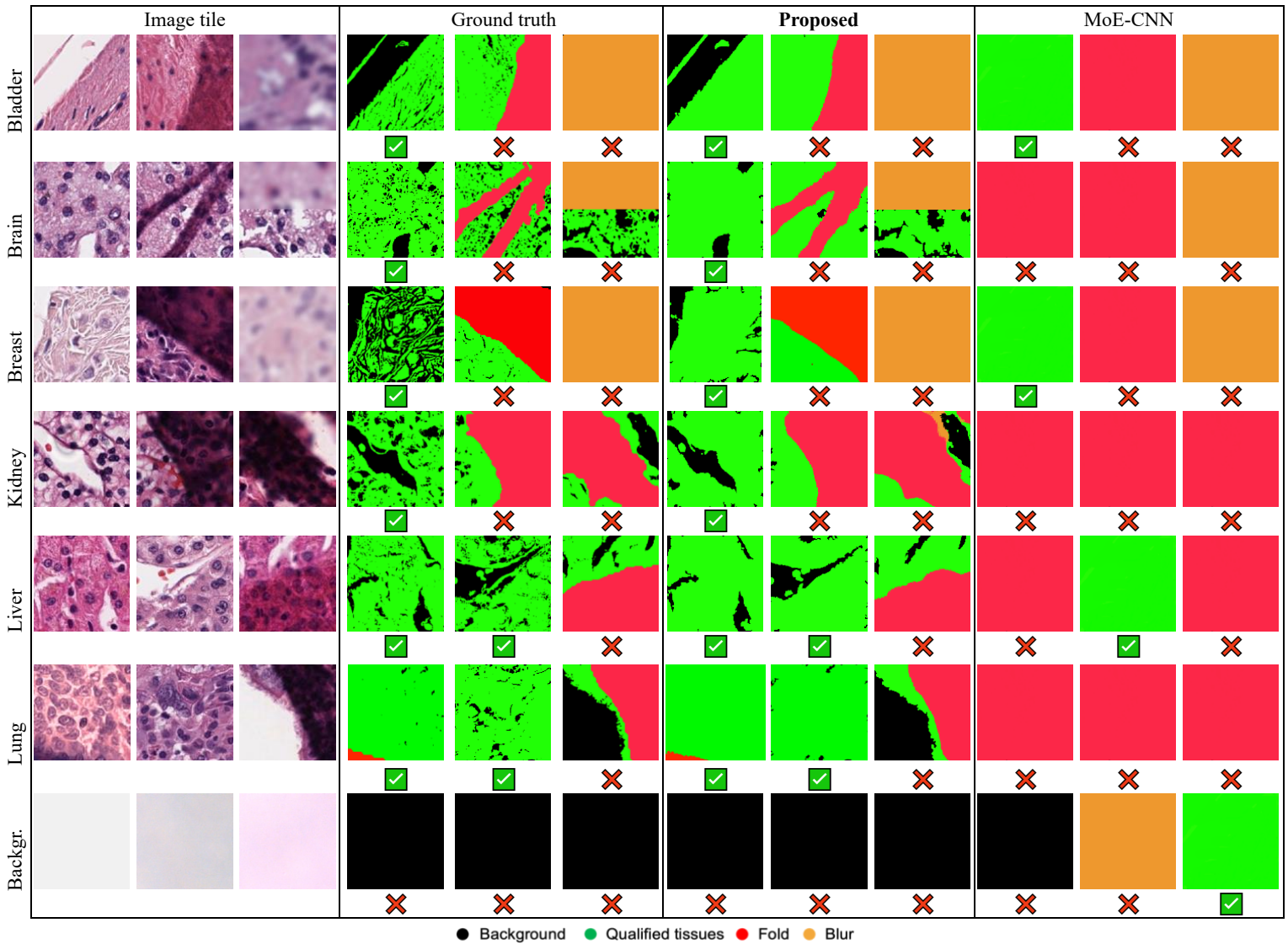


Fig. 5. Comparison of tile segmentation and classification between the proposed WSI-QA pipeline and the state-of-the-art method, MoE-CNN. The image tiles are taken from six different organs (bladder, brain, breast, kidney, liver, lung), as well as background-only tiles. Ground truth annotations are presented alongside model predictions, with tiles labeled as either ✓ (qualified) or ✗ (unqualified). Correct classifications are indicated when the ground truth and prediction labels match.

REFERENCES

- [1] O. Elemento, C. Leslie, J. Lundin, and G. Tourassi, "Artificial Intelligence in Cancer Research, Diagnosis and Therapy," *Nat Rev Cancer*, vol. 21, no. 12, pp. 747–752, Dec. 2021, doi: 10.1038/s41568-021-00399-1.
- [2] J. van der Laak, G. Litjens, and F. Ciompi, "Deep Learning in Histopathology: the Path to the Clinic," *Nat Med*, vol. 27, no. 5, pp. 775–784, May 2021, doi: 10.1038/s41591-021-01343-4.
- [3] M. Rakaee et al., "Deep Learning Model for Predicting Immunotherapy Response in Advanced Non-Small Cell Lung Cancer", 2024, *JAMA Oncol*. doi:10.1001/jamaoncol.2024.5356.
- [4] Y. Yang, K. Sun, Y. Gao, K. Wang, and G. Yu, "Preparing Data for Artificial Intelligence in Pathology with Clinical-Grade Performance," *Diagnostics*, vol. 13, no. 19, pp. 3115–3115, Oct. 2023, doi: 10.3390/diagnostics13193115.
- [5] A. H. Song et al., "Artificial Intelligence for Digital and Computational Pathology," *Nature Reviews Bioengineering*, vol. 1, no. 12, pp. 930–949, Oct. 2023, doi: 10.1038/s44222-023-00096-8.
- [6] B. Schömig-Markiefka et al., "Quality Control Stress Test for Deep Learning-Based Diagnostic Model in Digital Pathology," *Modern Pathology*, vol. 34, no. 12, pp. 2098–2108, Dec. 2021, doi: 10.1038/s41379-021-00859-x.
- [7] A. I. Wright, C. M. Dunn, M. Hale, G. G. A. Hutchins, and D. E. Treanor, "The Effect of Quality Control on Accuracy of Digital Pathology Image Analysis," *IEEE J Biomed Health Inform*, vol. 25, no. 2, pp. 307–314, Feb. 2021, doi: 10.1109/JBHI.2020.3046094.
- [8] Md. Z. Hoque, A. Keskinarkaus, P. Nyberg, and T. Seppänen, "Stain Normalization Methods for Histopathology Image Analysis: A Comprehensive Review and Experimental Comparison," *Information Fusion*, vol. 102, no. 1, p. 101997, Feb. 2024, doi: 10.1016/j.inffus.2023.101997.
- [9] M. Salvi, U. R. Acharya, F. Molinari, and K. M. Meiburger, "The Impact of Pre- and Post-image Processing Techniques on Deep Learning Frameworks: A Comprehensive Review for Digital Pathology Image Analysis," *Comput Biol Med*, vol. 128, no. 1, pp. 104129–104129, Jan. 2021, doi: 10.1016/j.compbimed.2020.104129.

- [10] D. Gao, D. Padfield, J. Rittscher, and R. McKay, "Automated Training Data Generation for Microscopy Focus Classification," in *International Conference on Medical Image Computing and Computer-Assisted Intervention*, Berlin, Heidelberg: Springer, Jan. 2010, pp. 446–453. doi: 10.1007/978-3-642-15745-5_55.
- [11] H. Wu, J. H. Phan, A. K. Bhatia, C. A. Cundiff, B. M. Shehata, and M. D. Wang, "Detection of Blur Artifacts in Histopathological Whole-Slide Images of Endomyocardial Biopsies," in *2015 37th Annual International Conference of the IEEE Engineering in Medicine and Biology Society*, Milan: IEEE, Aug. 2015, pp. 727–730. doi: 10.1109/EMBC.2015.7318465.
- [12] N. Hashimoto, P. A. Bautista, M. Yamaguchi, N. Ohya, and Y. Yagi, "Referenceless Image Quality Evaluation for Whole Slide Imaging," *J Pathol Inform*, vol. 3, no. 1, p. 9, Jan. 2012, doi: 10.4103/2153-3539.93891.
- [13] S. Palokangas, J. Selinummi, and O. Yli-Harja, "Segmentation of Folds in Tissue Section Images," in *2007 29th Annual International Conference of the IEEE Engineering in Medicine and Biology Society*, Lyon, France: IEEE, Aug. 2007, pp. 5641–5644. doi: 10.1109/IEMBS.2007.4353626.
- [14] P. A. Bautista and Y. Yagi, "Detection of Tissue Folds in Whole Slide Images," in *2009 Annual International Conference of the IEEE Engineering in Medicine and Biology Society*, Minneapolis, Minnesota: IEEE, Sep. 2009, pp. 3669–3672. doi: 10.1109/IEMBS.2009.5334529.
- [15] S. Kothari, J. H. Phan, and M. D. Wang, "Eliminating tissue-Fold Artifacts in Histopathological Whole-Slide Images for Improved Image-Based Prediction of Cancer Grade," *J Pathol Inform*, vol. 4, no. 1, pp. 22–22, Jan. 2013, doi: 10.4103/2153-3539.117448.
- [16] E. Mercan, S. Aksoy, L. G. Shapiro, D. L. Weaver, T. T. Brunyé, and J. G. Elmore, "Localization of Diagnostically Relevant Regions of Interest in Whole Slide Images: a Comparative Study," *J Digit Imaging*, vol. 29, no. 4, pp. 496–506, Aug. 2016, doi: 10.1007/s10278-016-9873-1.
- [17] A. Janowczyk, R. Zuo, H. Gilmore, M. Feldman, and A. Madabhushi, "HistoQC: An Open-Source Quality Control Tool for Digital Pathology Slides," *JCO Clin Cancer Inform*, vol. 1, no. 3, pp. 1–7, Dec. 2019, doi: 10.1200/CCI.18.00157.
- [18] T. Albuquerque, A. Moreira, and J. S. Cardoso, "Deep Ordinal Focus Assessment for Whole Slide Images," in *2021 IEEE/CVF International Conference on Computer Vision Workshops*, Montreal, BC, Canada: IEEE, Oct. 2021, pp. 657–663. doi: 10.1109/ICCVW54120.2021.00079.
- [19] T. Kohlberger *et al.*, "Whole-Slide Image Focus Quality: Automatic Assessment and Impact on AI Cancer Detection," *J Pathol Inform*, vol. 10, no. 1, p. 39, Jan. 2019, doi: 10.4103/jpi.jpi_11_19.
- [20] M. Babaie and H. R. Tizhoosh, "Deep Features for Tissue-Fold Detection in Histopathology Images," 1st ed., vol. 11435, Warwick, United Kingdom: Springer Verlag, 2019, pp. 125–132. doi: 10.1007/978-3-030-23937-4_15.
- [21] N. Kanwal, T. Eftestøl, F. Khoraminia, T. C. M. Zuiverloon, and K. Engan, "Vision Transformers for Small Histological Datasets Learned Through Knowledge Distillation," in *Pacific-Asia Conference on Knowledge Discovery and Data Mining*, Osaka, Japan: Springer, Cham, May 2023, pp. 167–179. doi: 10.1007/978-3-031-33380-4_13.
- [22] N. Kanwal, S. Fuster, F. Khoraminia, T. C. M. Zuiverloon, C. Rong, and K. Engan, "Quantifying the Effect of Color Processing on Blood and Damaged Tissue Detection in Whole Slide Images," in *2022 IEEE 14th Image, Video, and Multidimensional Signal Processing Workshop (IVMSP)*, Nafplio, Greece: IEEE, Jun. 2022, pp. 1–5. doi: 10.1109/IVMSP54334.2022.9816283.
- [23] N. Kanwal *et al.*, "Equipping Computational Pathology Systems with Artifact Processing Pipelines: A Showcase for Computation and Performance Trade-offs," *ArXiv Preprint:2403.07743*, vol. 1, no. 1, Mar. 2024.
- [24] N. Kanwal, M. López-Pérez, U. Kiraz, T. C. M. Zuiverloon, R. Molina, and K. Engan, "Are You Sure it's an Artifact? Artifact Detection and Uncertainty Quantification in Histological Images," *Computerized Medical Imaging and Graphics*, vol. 112, no. 1, p. 102321, Mar. 2024, doi: 10.1016/j.compmedimag.2023.102321.
- [25] M. Rakae *et al.*, "Association of Machine Learning-Based Assessment of Tumor-Infiltrating Lymphocytes on Standard Histologic Images With Outcomes of Immunotherapy in Patients With NSCLC," *JAMA Oncol*, vol. 9, no. 1, pp. 51–51, Jan. 2023, doi: 10.1001/jamaoncol.2022.4933.
- [26] M. Rakae *et al.*, "Machine Learning-Based Immune Phenotypes Correlate with STK11/KEAP1 Co-mutations and Prognosis in Resectable NSCLC: a Sub-study of the TNM-I Trial," *Annals of Oncology*, vol. 34, no. 7, pp. 578–588, Jul. 2023, doi: 10.1016/j.annonc.2023.04.005.
- [27] National Cancer Institute, "TCGA Dataset," https://portal.gdc.cancer.gov/analysis_page?app=Projects.
- [28] QuPath, "QuPath Software," 2024, <https://qupath.readthedocs.io/en/stable/>: QuPath 0.5.1.
- [29] V. Abrol, S. Dhalla, S. Gupta, S. Singh, and A. Mittal, "An Automated Segmentation of Leukocytes Using Modified Watershed Algorithm on Peripheral Blood Smear Images," *Wirel Pers Commun*, vol. 131, no. 1, pp. 197–215, Jul. 2023, doi: 10.1007/s11277-023-10424-1.
- [30] Open Source Computer Vision, "Otsu's Binarization," 2024, https://docs.opencv.org/4.x/d7/d4d/tutorial_py_thresholding.html.
- [31] Scikit Image, "Remove Small Objects," 2024, https://scikit-image.org/docs/stable/api/skimage.morphology.html#skimage.morphology.remove_small_objects.
- [32] Scikit Image, "Binary Dilation," 2024, <https://scikit-image.org/docs/stable/api/skimage.morphology.html#module-skimage.morphology>.
- [33] Pytorch, "Torch Multiprocessing," 2024, <https://pytorch.org/docs/stable/notes/multiprocessing.html>.
- [34] L. Wang *et al.*, "DHU-net: Dual-branch Hierarchical Global-Local Fusion Network for Whole Slide Image Segmentation," *Biomed Signal Process Control*, vol. 85, no. 1, pp. 104976–104976, Aug. 2023, doi: 10.1016/j.bspc.2023.104976.
- [35] Weights & Biases, "Weights & Biases Visualization Tools," 2024, <https://docs.wandb.ai>.
- [36] PyTorch, "PyTorch Transformation and Augmentation Techniques," 2024, <https://pytorch.org/vision/main/transforms.html>.
- [37] M. Sokolova and G. Lapalme, "A Systematic Analysis of Performance Measures for Classification Tasks," *Inf Process Manag*, vol. 45, no. 4, pp. 427–437, Jul. 2009, doi: 10.1016/j.ipm.2009.03.002.
- [38] P. Isola, J.-Y. Zhu, T. Zhou, and A. A. Efros, "Image-to-Image Translation with Conditional Adversarial Networks," in *2017 IEEE Conference on Computer Vision and Pattern Recognition (CVPR)*, Honolulu, HI, USA: IEEE, Jul. 2017, pp. 5967–5976. doi: 10.1109/CVPR.2017.632.
- [39] S. Mukhopadhyay *et al.*, "Diffusion Models Beat GANs on Image Classification," *ArXiv*, pp. 1–1, Jul. 2023.